Iron(II) Formate $[Fe(O_2CH)_2]\cdot 1/3HCO_2H$: A Mesoporous Magnet − Solvothermal Syntheses and Crystal Structures of the Isomorphous Framework Metal(II) Formates $[M(O_2CH)_2]\cdot n$(Solvent) (M = Fe, Co, Ni, Zn, Mg)

Martin Viertelhaus,[a] Peter Adler,[a] Rodolphe Clérac,[b] Christopher E. Anson,[a] and Annie K. Powell*[a]

Keywords: Iron / Solvothermal synthesis / Framework material / Magnetic properties / Mössbauer spectroscopy

Recrystallisation of iron(II) formate dihydrate from formic acid under solvothermal conditions results in single-crystals of the iron(II) formate, α-$Fe(O_2CH)_2\cdot 1/3HCO_2H$. The crystal structure of this phase has been determined by X-ray diffraction and reveals an open framework structure with formic acid molecules occupying channels in the lattice which is stable even after removal of the solvent molecules. Magnetic susceptibility and Mössbauer measurements show that the compound undergoes 3D magnetic ordering below $T_C = 16$ K. α-$Fe(O_2CH)_2\cdot 1/3HCO_2H$ and the corresponding magnesium, cobalt, nickel and zinc formates form an isomorphous series. In contrast to the iron compound, the magnetic behaviour of the cobalt analogue is dominated by antiferromagnetic interactions.

Introduction

The versatility of carboxylate anions as units for ligating and connecting metal centres has led to extensive research on the structures and properties of carboxylato complexes. Among the many fascinating examples in the literature are molecular entities such as the well-known oxo-centred trinuclear complexes,[1] the "Single Molecule Magnet" $[Mn_{12}O_{12}(O_2CCH_3)_{16}(OH_2)_4]\cdot 4H_2O\cdot 2CH_3CO_2H$ and related clusters[2,3] as well as extended systems, often produced using solvothermal synthesis, where the presence or absence of template molecules leads to open framework structures such as $Mn_4(PO_4)_2(C_2O_4)(H_2O)_2$[4] or very densely packed materials such as β-$Mn(O_2CMe)_2$.[5] Of particular current interest is the possibility of synthesising dual functionality materials where, for example, a mesoporous structure could also display a second useful physical property, such as cooperative magnetic behaviour.[6] These could be used to isolate and store paramagnetic molecules including gases such as dioxygen. Of the compounds which have so far been shown to display magnetic ordering and a microporous structure,[6b−6g] only $Co_3[Co(CN)_5]_2$,[6a] has displayed hysteresis and can be described as a ferrimagnet with $T_N = 38$ K. It has a defect Prussian Blue structure on the basis of its X-ray powder pattern.

We have been exploring the crystal structures and properties of compounds with the formate anion as a carboxylate linking unit, produced using solvothermal conditions.[7] Although the formate anion is the simplest carboxylate, most compounds described in the literature which have been structurally characterised using single-crystal X-ray diffraction have been synthesised using acetates and higher homologues. For most transition metal(II) formates, only single-crystal structure determinations for the dihydrates have been reported. The divalent 3*d*-transition metals, together with magnesium and cadmium, form an isomorphous series of metal(II) formate dihydrates.[8] Single-crystal structures of anhydrous diformates of these metals have only been determined for copper,[9] cadmium[10] and manganese.[11] This lack of knowledge concerning the structures of anhydrous transition metal(II) formates is comparable with that for the corresponding anhydrous nitrates or acetates[11] and is in contrast to the extensive research on the properties of such materials characterised only by X-ray powder diffraction (Mg,[12] Mn,[13] Fe,[14] Co,[15] Ni,[16] Zn[17]) and IR spectroscopy.[18] The kinetics and thermodynamics of the dehydration reactions of the dihydrates and the rehydration of the anhydrous products of dehydration[19] have been studied as well as the use of the dihydrates as precursors for dehydrogenation catalysts.[20] As far as the anhydrous metal(II) formates, $M(O_2CH)_2$, are concerned the Cu^{II} and Cd^{II} examples were synthesised at temperatures around 60−80 °C by slow evaporation of the solvent consisting of a mixture of water and formic acid. Single-crystals of other anhydrous

[a] Institut für Anorganische Chemie, Universität Karlsruhe, Engesser Str. 15, Geb. 30.45, 76128 Karlsruhe, Germany
Fax: (internat.) + 49-721-608-8142
E-mail: powell@chemie.uni-karlsruhe.de
[b] Centre de Recherche Paul Pascal, CNRS UPR-8641, 115 Avenue Dr. A. Schweitzer, 33600 Pessac, France
Supporting information for this article is available on the WWW under http://www.eurjic.org or from the author.

  DOI: 10.1002/ejic.200400395

formates are not available using this synthetic route, although Vassileva and Karapetkova were able to isolate anhydrous formates of manganese, iron and zinc under ambient conditions as microcrystalline solids.[21]

We recently described the single-crystal X-ray structure of the new anhydrous formate $[Mn(O_2CH)_2]$ which can be prepared either using modified solvothermal conditions or by an unusual topotactic solid-state dehydration of the corresponding dihydrate.[11] As part of our survey of metal(II) formates we also found an isomorphous series of mesoporous framework compounds of general formula $M(O_2CH)_2\cdot 1/3HCO_2H$ for M = Fe, Co, Ni, Zn and Mg,[7] the synthesis, structures and properties of which we report here with particular reference to the Fe^{II} compound and its magnetic behaviour. Whilst we were investigating these magnetic properties, the structures of $Mn(O_2CH)_2\cdot 1/3C_4H_8O_2$ and $Mn(O_2CH)_2\cdot 1/3CH_3OH\cdot 1/3H_2O$ were reported both of which are isomorphous compounds with the same metal-formate framework we have observed.[22]

Results and Discussion

Syntheses

Recrystallisation of iron(II) formate dihydrate, $Fe(O_2CH)_2\cdot 2H_2O$, from formic acid under solvothermal conditions yields transparent green crystals of α-$Fe(O_2CH)_2\cdot 1/3HCO_2H$, suitable for X-ray diffraction (Scheme 1). The crystal structure was determined at 200 K and crystallographic details are summarised in Table 1. The same product, with a higher degree of purity but in a microcrystalline form, can be obtained in quantitative yield using milder conditions. Vassileva and Karapetkova had already observed this anhydrous iron(II) formate phase in the ternary system $Fe(O_2CH)_2-H_2O-HCO_2H$ at 25 °C with concentrations of formic acid higher than 83%.[21] The powder diffraction pattern of this product was different from the powder pattern of the product from direct dehydration of $Fe(O_2CH)_2\cdot 2H_2O$.[23] Vassileva and Karapetkova called their product anhydrous iron formate. As will be shown below, they had not prepared a pure formate free of solvent but, rather, an open framework structure with formic acid molecules occupying channels in the lattice. Since it is possible to desolvate the crystals, we refer to the synthesised or primary product $Fe(O_2CH)_2\cdot 1/3HCO_2H$ as α-FeFA·$1/3HCO_2H$. The stable crystalline network structure with-

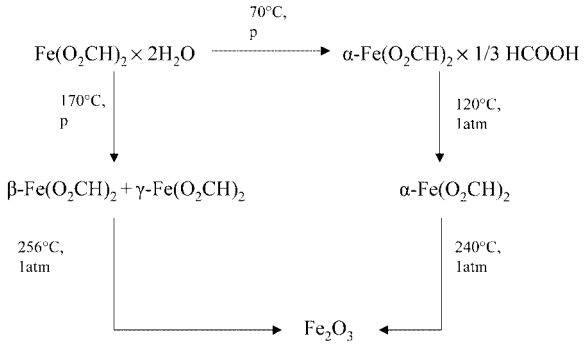

Scheme 1. Products and derivatives of mild solvothermal recrystallisation of iron(II) formate dihydrate; p = autogenous pressure of formic acid under solvothermal conditions; further heating of the amorphous Fe_2O_3 leads to haematite (α-Fe_2O_3)

Table 1. Crystal data and details of structural refinements

	α-FeFA·$1/3HCO_2H$	α-CoFA·$1/3HCO_2H\cdot 1/3(H_2O)$	α-ZnFA·$1/3HCO_2H$
Formula	$C_{2.33}H_{2.67}FeO_{4.67}$	$C_{2.33}H_{3.33}CoO_5$	$C_{2.33}H_{2.67}O_{4.67}Zn$
Molecular mass	161.23	170.31	170.75
Crystal system	monoclinic	monoclinic	monoclinic
Space group	$P2_1/n$ (no. 14)	$P2_1/n$ (no. 14)	$P2_1/n$ (no. 14)
Temperature [K]	200(2)	200(2)	200(2)
a (Å)	11.4446(10)	11.2727(9)	11.3407(9)
b (Å)	9.9304(9)	9.8335(6)	9.7856(8)
c (Å)	14.6192(15)	14.4249(12)	14.4334(13)
β (°)	91.423(11)	91.242(7)	91.449(10)
Volume (Å^3)	1661.0(3)	1598.6(2)	1601.2(2)
Z	12	12	12
D_c [g cm^{-3}]	1.934	2.106	2.125
μ [Mo-K_α] [mm^{-1}]	2.652	3.154	4.527
Crystal dimensions (mm)	0.20 × 0.20 × 0.05	0.10 × 0.10 × 0.05	0.50 × 0.40 × 0.20
Crystal shape	green plate	pink plate	colourless block
$2\theta_{max}$	52.3°	54.2°	52.4°
Reflections measured	8198	10340	10183
Independent reflections	3179	3367	3151
R_{int}	0.0889	0.0315	0.0340
Reflections with [$I > 2\sigma(I)$]	2428	3137	2899
wR_2 (all data)	0.1692	0.1412	0.1168
Goodness of fit S	0.984	1.053	1.001
R_1 [$I > 2\sigma(I)$]	0.0602	0.0497	0.0411
Parameters/restraints	235/10	245/9	257/7
Max. diff. peak/hole [e·Å^{-3}]	+1.23/−0.89	+1.12/−1.27	+0.82/−1.05

Table 2. Unit cell parameters for the isomorphous series of formates (the compounds crystallise in space group $P2_1/n$, no.14)

Compound	ref.	a (Å)	b (Å)	c (Å)	β (°)	V (Å^3)	T (K)
α-MgFA·1/3(HCO_2H)	[a]	11.350(8)	9.876(4)	14.541(12)	91.51(5)	1629(2)	300
α-MnFA·1/3dioxane	[22a]	11.715(2)	10.248(2)	15.159(3)	91.81(2)	1819.0(7)	223
α-MnFA	[22a]	11.720(1)	10.207(1)	14.956(2)	91.44(1)	1788.6(3)	223
α-MnFA·1/3CH_3OH·1/3H_2O[b]	[22b]	11.650(1)	10.128(1)	14.861(2)	91.670(3)	1752.6(3)	180
α-FeFA·1/3HCO_2H	[a]	11.4446(10)	9.9304(9)	14.6192(15)	91.423(11)	1661.0(3)	200
α-CoFA·1/3HCO_2H·1/3H_2O	[a]	11.2727(9)	9.8335(6)	14.4249(12)	91.242(7)	1598.6(2)	200
α-NiFA·$x$$HCO_2H$·$y$$H_2O$	[a]	11.1586(6)	9.7789(4)	14.3333(8)	91.447(4)	1563.53(10)	300
α-ZnFA·1/3HCO_2H·1/3H_2O	[a]	11.3407(9)	9.7856(8)	14.4334(13)	91.449(10)	1601.2(2)	200

[a] This work. [b] This structure was published in the alternative space group setting $P2_1/c$. The appropriately transformed cell is given in the above table for consistency with the other structures.

out solvate molecules is thus α-FeFA. In the course of our work, we have also characterised two further anhydrous and solvent-free iron(II) formates, namely β- and γ-FeFA (see Scheme 1) which will be published separately.[24] The three different compounds thus necessitate use of the prefixes α, β and γ.

Similar synthetic methods were used to obtain α-MFA·1/3HCO_2H (M = Zn, Mg) and α-CoFA·1/3HCO_2H·1/3H_2O. Although the magnesium compound could only be obtained as a microcrystalline material, the solvent molecules could be identified from the IR spectrum. The nickel analogue could also be prepared but was highly unstable when removed from the mother liquor. The unit cell could be determined from a sample prepared in situ in a glass capillary, demonstrating that the nickel complex is indeed isomorphous with the other compounds but the precise solvent content of the crystals of the nickel formate remains uncertain. For convenience, the unit cell parameters for all the compounds reported here, as well as the recently reported Mn^{II} complexes,[22] are listed in Table 2.

Framework Structure

α-Fe(O_2CH)$_2$·1/3HCO_2H crystallises in the monoclinic space group $P2_1/n$ with $Z = 12$. Selected geometrical parameters are listed in Table 3. The structure of the isomorphous Mn^{II} analogue has been discussed[22] with reference to its open framework structure, where it was described as a diamondoid network of metal centres, although the channels only run through the network in one direction, rather than in the four directions implied by this description. Since we were particularly interested in investigating the magnetic behaviour of the system, which turned out to be fairly complicated, our structural description concentrates on the metal ion coordination spheres and the chemical links between the metal centres which could mediate possible magnetic interactions.

The asymmetric unit of α-FeFA·1/3HCO_2H contains four independent iron centres with Fe(1) and Fe(2) on general positions, and Fe(3) and Fe(4) representing inversion centres. All four have distorted octahedral coordination spheres of oxygen atoms from formate ions with angles in the ranges 78.00−97.34° and 164.19−180° (Table 3). Each of the six independent formate ligands forms a μ_3-(*syn,syn-anti*) carboxylate bridge between three Fe centres and for convenience the numbering is such that the odd-numbered oxygen forms the (μ_2-η^1) bridge, while the even-numbered oxygen is monodentate. The Fe−O bond lengths (Table 3) are, on average, slightly longer for the bridging oxygen atoms being in the range 2.080(4)−2.174(4) Å (mean value 2.142 Å), whereas those involving a monodentate oxygen lie in the range 2.072(4)−2.154(4) Å (mean 2.098 Å).

The framework structure is generated firstly from chains of Fe(1) and Fe(2) running along the 2_1-screw axes {Fe(1)−Fe(2)−Fe(1a)−Fe(2a)...} (Figure 1). Within the chains, pairs of iron atoms are linked by one *syn*,*syn*-for-

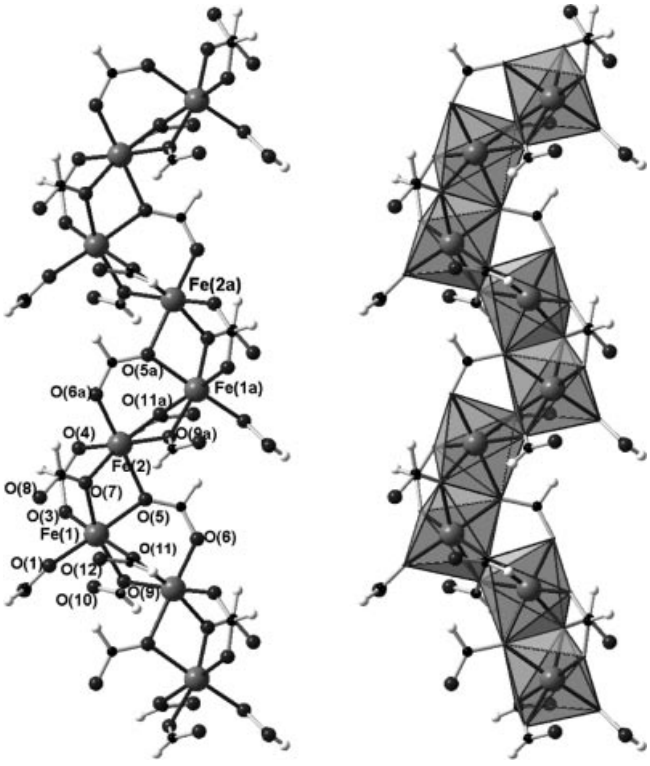

Figure 1. The serpentine chain made up of Fe(1) and Fe(2) running along the 2_1-screw axis parallel to the crystal b-axis and projected onto the {1 0 0} plane showing the formate bridges between adjacent iron centres and the edge-sharing octahedral coordination polyhedra of the iron centres; symmetry code: $a = -x + 1/2$, $y - 1/2$, $-z + 1/2$; Fe − large mid-grey circles, O − dark grey circles; C − small black circles; H − very small white circles

Table 3. M−O distances, M−O−M angles and M···M separations

Distances (Å) and angles (°)	α-FeFA·1/3HCO_2H	α-CoFA·1/3HCO_2H·1/3H_2O	α-ZnFA·1/3HCO_2H
M(1)−O(1)	2.080(4)	2.048(3)	2.040(2)
M(1)−O(3)	2.108(4)	2.071(3)	2.070(2)
M(1)−O(5)	2.134(4)	2.091(3)	2.109(2)
M(1)−O(7)	2.155(4)	2.116(3)	2.116(2)
M(1)−O(9)	2.159(4)	2.116(3)	2.115(2)
M(1)−O(11)	2.124(4)	2.086(3)	2.111(2)
M(2)−O(4)	2.069(4)	2.042(3)	2.033(2)
M(2)−O(5)	2.145(4)	2.108(3)	2.138(2)
M(2)−O(6^{i})	2.072(4)	2.051(3)	2.023(3)
M(2)−O(7)	2.145(4)	2.106(3)	2.092(2)
M(2)−O(9^{i})	2.154(4)	2.122(3)	2.164(2)
M(2)−O(11^{i})	2.120(4)	2.051(3)	2.083(2)
M(3)−O(1)	2.175(4)	2.123(3)	2.127(2)
M(3)−O(8)	2.082(4)	2.058(3)	2.066(3)
M(3)−O(12)	2.120(5)	2.098(3)	2.090(3)
M(4)−O(2)	2.104(5)	2.078(3)	2.072(3)
M(4)−O(3)	2.160(4)	2.114(3)	2.118(2)
M(4)−O(10)	2.115(5)	2.078(3)	2.077(3)
Mean M−O(μ_1)	2.098	2.072	2.067
Mean M−O(μ_2)	2.142	2.099	2.108
M(1)−O(1)−M(3)	113.53(17)	114.79(12)	115.50(11)
M(1)−O(3)−M(4)	111.84(17)	112.72(13)	112.27(11)
M(1)−O(5)−M(2)	96.71(16)	97.37(10)	96.49(9)
M(1)−O(7)−M(2)	96.09(16)	96.69(10)	97.65(10)
M(1)−O(9)−M(2^{ii})	97.28(16)	97.32(11)	97.52(9)
M(1)−O(11)−M(2^{ii})	99.42(17)	99.70(11)	100.19(10)
M(1)···M(2)	3.1973(10)	3.1539(7)	3.1680(6)
M(1)···M(2^{ii})	3.2367(11)	3.1874(7)	3.2172(5)
M(1)···M(4)	3.5346(9)	3.4840(5)	3.4772(5)
M(1)···M(3)	3.5592(9)	3.5137(5)	3.5244(5)
M(2)···M(2^{ii})	5.2958(7)	5.2311(4)	5.2362(5)
M(3)···M(2^{ii})	5.3758(10)	5.3008(6)	5.3269(7)
M(2)···M(4)	5.5364(8)	5.4598(6)	5.4700(5)
M(2)···M(3)	5.5847(9)	5.5159(6)	5.5161(5)
M(4)···M(2^{ii})	5.6136(10)	5.5205(7)	5.5638(7)
M(3)···M(4)	5.7223(5)	5.6363(5)	5.6704(5)
Symmetry equivalents:	i: $-x + 1/2, y + 1/2, -z + 1/2$ ii: $-x + 1/2, y - 1/2, -z + 1/2$		

mate bridge with O(5) and O(7) joining Fe(1) and Fe(2), and two μ-bridging oxygen atoms with O(9) and O(11) joining Fe(1) and Fe(2a). The coordination polyhedra of Fe(1) and Fe(2) can thus be described as edge-sharing octahedra, with the shared edges defined by these four oxygens (Figure 1). This leads to two alternating crystallographically distinct, although geometrically rather similar Fe···Fe linkages. Of particular interest in terms of the magnetic behaviour is that the Fe−O−Fe angles at O(5), O(7), O(9) and O(11) all lie in the range 96.08−99.42° (Table 3) and might therefore be expected to mediate rather similar magnetic interactions (vide infra).

The chains are cross-linked via further Fe^{II} centres, namely Fe(3) and Fe(4) in the *ac*-plane (Figure 2 and Figure 3). The linkages from Fe(1) to either Fe(3) or Fe(4) both involve a single μ-oxygen bridge [O(1) and O(3), respectively] and two *syn*,*syn*-formate bridges. In contrast, Fe(2) is only linked to Fe(3) and Fe(4) through single *syn*,*anti*-formate bridges. The Fe−O−Fe angles at the bridging oxygens O(1) and O(3) are similar and significantly larger than those forming the bridges within the chains at 111.84° and 113.54°, respectively, and could thus mediate magnetic interactions similar to each other but significantly different from the intrachain linkages.

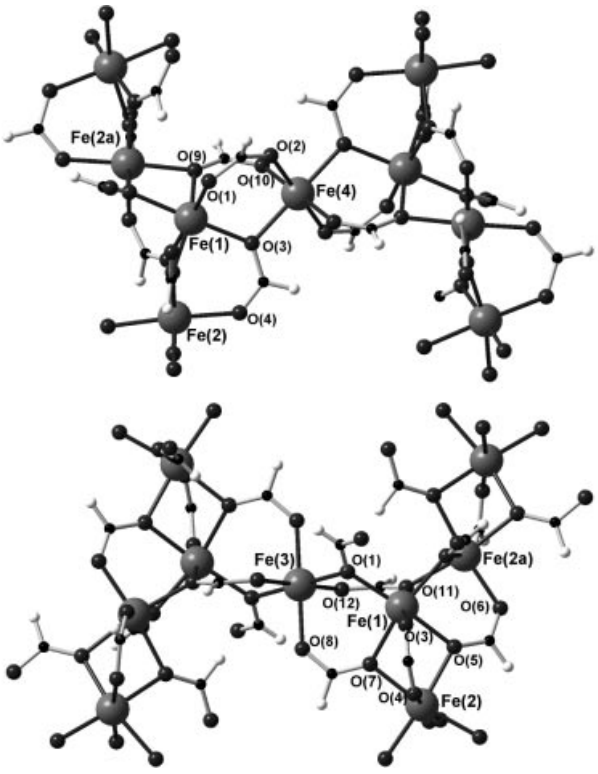

Figure 2. The interchain linkages through Fe(4) (upper) and through Fe(3) (lower); atom key and symmetry code as in Figure 1

Of further interest in terms of the magnetic behaviour is the presence of any distortion in the coordination spheres of the Fe^{II} centres which can affect the zero-field splitting and ground state term. Fe(3) and Fe(4) each show slight tetragonal elongations along one axis, with Fe−O distances of 2.175(4) and 2.159(4) Å, respectively, compared with the shorter distances in the range 2.082(4) −2.120(4) Å. However, Fe(1) and Fe(2) show no such pattern and indeed for Fe(2) the longest Fe−O distance is *trans* to the shortest.

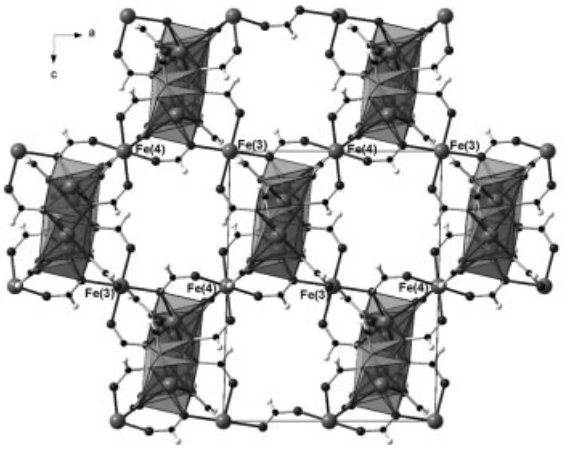

Figure 3. The structure of α-FeFA·1/3HCO_2H viewed along the *b*-direction showing its channel structure; Fe(1) and Fe(2), which form the chains bridged by pairs of μ-oxygen bridges, are shown as coordination polyhedra; Fe(3) and Fe(4) and their symmetry-equivalents, which form linkages between the chains, are shown as conventional atoms; formic acid molecules inside the channels are omitted for clarity

Mesoporous Behaviour

An examination of the stabilised open framework structure of α-FeFA·1/3HCO_2H using PLATON[25] showed that the accessible volume of the channels amounts to 505 $Å^3$ per unit cell, or 30.5% of the unit cell volume which is in good agreement with the values for the manganese compounds.[22] It has been shown that the manganese-based-framework can accommodate a wide variety of guest molecules. The channels in the synthesised iron compound contain formic acid molecules. In the structure, these solvent molecules are twofold disordered with the overlapping half-molecules occupying one general position. This results in one third of a formic acid molecule per iron atom in the formula, i.e. α-FeFA·1/3HCO_2H. The presence of formic acid in the lattice was confirmed by the IR spectrum (Table 4). In addition to the expected bands from the for-

Table 4. IR absorptions (KBr, cm^{-1}) for the complexes presented in this work (s strong, w weak, sh shoulder, vw very weak, br broad, m medium, n.o. not observed)

Vibration[42]	α-FeFA·1/3HCO_2H	α-CoFA·1/3HCO_2H·1/3H_2O	α-ZnFA·1/3HCO_2H	α-MgFA·1/3HCO_2H
ν(OH), HCO_2H	3432 mw, br	3347 m	3434 m, br	3466 mw, br
ν(OH), H_2O	−	3300 s, 3221 m	−	−
νCH	2925 m, 2888 m	2929 m, 2902 m	2926 m	2932 m
ν(C=O), HCO_2H	1742 mw,	1724 mw, 1665 sh	1728 mw	1731 m
νCO, asym.	1646 s, 1610 vs, 1586 vs	1644 sh, 1582 vs	1650 sh, 1600 sh, 1581 vs	1670 ms, 1642 vs, 1607 vs
δ(OCO)	1400 m, 1389 m	1397 s, 1378 s	1397 m, 1369 sh	1416 m, 1407 mw
νCO, sym.	1331 s	1357 s, 1328 m	1352 s, 1325 s	1340 s
ν(C−O), HCO_2H	1163 vw, 1144 w	1191 vw	1188 w	1188 w
γ(CH)	1066 vw	n.o.	n.o.	1076 vw
δ(OCO), sym.	781 m	788 m, 766 m	787 m	791 m

mate ligands, a single band at 3430 cm^{-1}, a stronger band at 1742 cm^{-1} and a pair of bands at 1163 and 1144 cm^{-1} can be assigned to free formic acid molecules.[26] There was no evidence in the spectrum for the presence of water molecules. The stoichiometry of the formic acid can be verified by STA-experiments on a briefly-dried sample from the solvothermal synthesis. The sample loses mass in several unresolved processes between room temperature and 160 °C. The overall mass loss for these steps is 9.2% which is in good agreement with the theoretical mass loss of 9.5% for $1/3HCO_2H$ per iron atom to give α-FeFA. Between 160 and 270 °C, α-FeFA decomposes exothermally to amorphous Fe_2O_3 with a further mass loss of 39.7% (calcd. 40.9%).

Pure desolvated α-FeFA can be obtained by heating the powder α-FeFA·$1/3HCO_2H$ to 120 °C for several hours. The desolvation can be monitored by X-ray powder diffraction. For example, on heating the sample, the 002 reflection increases in intensity, whereas the $\bar{1}11$, 200 and 112 reflections decrease (Figure 4). To further verify this, the powder pattern calculated from the crystal structure of α-FeFA·$1/3HCO_2H$ was compared with the pattern calculated from the same structure with the atoms of the formic acid molecule removed. As can be seen in Figure 4, these patterns show the same trends as the experimentally measured patterns and that calculated from the structure with the formic acid atoms deleted is essentially identical to the final experimental powder pattern in which all peaks could be indexed. The structural framework is thus not merely stable to removal of the solvent but also maintains its structure with minimal changes in geometry. In contrast, if a sample of α-FeFA·$1/3HCO_2H$ is kept in vacuo for several days, no significant change in the powder diffraction pattern can be observed, indicating that heating is necessary to remove the formic acid solvent molecules.

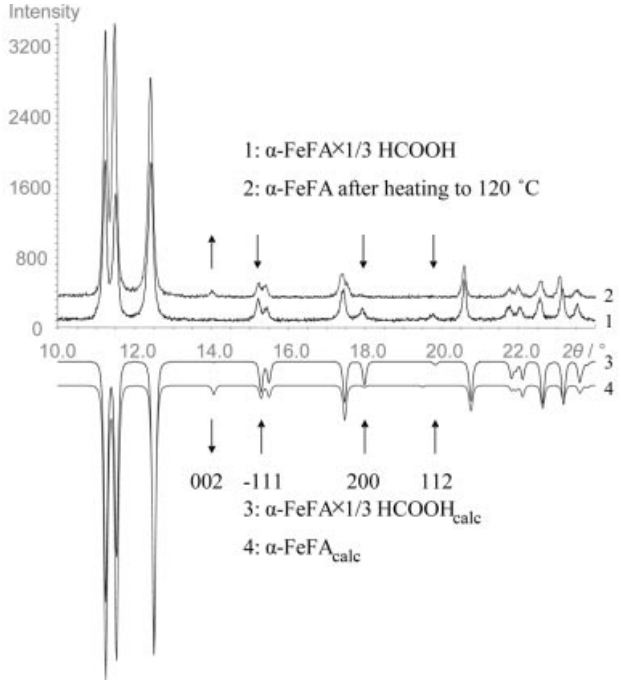

Figure 4. X-ray powder diffraction with Co-$K\alpha_1$ radiation shows the stability of the channel structure of α-FeFA on removal of the solvent molecules; significant changes in intensities on heating are marked with arrows; for comparison the calculated patterns are shown

The IR spectra of the magnesium and zinc formates show no evidence for the presence of water molecules in the lattices. STA results for the zinc and magnesium compounds indicate mass losses of 9.1 and 9.7%, respectively, in agreement with the theoretical value for loss of $1/3HCO_2H$ per metal atom (9.0 and 10.7%, respectively). We have therefore formulated both these compounds analogously to the iron formate, i.e. as α-MFA·$1/3HCO_2H$ (M = Zn, Mg). In contrast, the IR spectra of the cobalt analogue show, in addition to bands from the bridging formate ligands and formic acid solvent molecules as found for the other three complexes, two additional bands in the 3300−3200 cm^{-1} region which indicate that water molecules are present in the channels in addition to formic acid. The expected band at ca. 1630 cm^{-1} for the deformation mode of water is obscured by the very strong formate bands. The additional presence of water in the solvent lattice was confirmed by the STA results. The mass loss on heating to 140 °C is significantly higher than for the iron complex with a mean value of 13.2% which can be compared with the calculated mass losses per Co atom of 9.1% for $1/3HCO_2H$ and 12.5% for $1/3HCO_2H + 1/3H_2O$. In the crystal structure, the solvent could readily be refined as a slightly disordered formic acid molecule and a water molecule disordered between two adjacent sites. We have thus formulated the cobalt formate as α-CoFA·$1/3HCO_2H\cdot 1/3H_2O$ and note the similar formulation of MnFA·$1/3CH_3OH\cdot 1/3H_2O$ found for the compound described in ref.[22b]

Magnetic Properties

The χT product of α-FeFA·$1/3HCO_2H$ shown in Figure 5 continuously increases from 4.72 emu K mol^{-1} at 300 K up to a value of 28 emu K mol^{-1} at 20 K. Above this temperature the paramagnetic behaviour can be satisfactorily reproduced by a Curie−Weiss law with a Curie constant of 4.5 emu K mol^{-1}, corresponding to an average g value of 2.45, in agreement with typical values for high spin Fe^{II} metal ions in a distorted octahedral geometry.[27] The positive

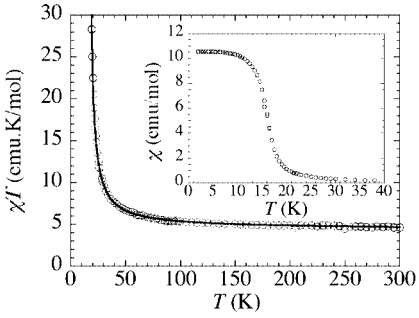

Figure 5. Temperature dependence of the χT product ($\chi = M/H$ per Fe^{II}) at 1000 Oe for α-FeFA·$1/3HCO_2H$; the solid line corresponds to the best fit obtained with the Curie−Weiss law with C = 4.5 emu K/mol, θ = +16 K and χ_{dia} = −3.5 10^{-4} emu/mol

Weiss constant of +16 K is indicative of dominant ferromagnetic interactions within the framework. Below 20 K, the susceptibility, χ, increases dramatically and reaches a saturation value of 10.6 emu mol^{-1} at around 5 K. This behaviour is typically associated with the onset of spontaneous magnetisation and therefore with the stabilisation of magnetic 3D order. Heat capacity measurements made on a pressed pellet of α-FeFA·1/3HCO_2H confirmed the magnetic transition observed (Figure S1). A lambda peak indicative of a second order phase transition was obtained at 16 K.

In order to obtain more insight into the low temperature magnetic phase, the field dependence of the magnetisation was investigated. As shown in Figure 6, the magnetic moment (M) increases very rapidly in small magnetic fields below 15 K. This increase slows at around 2000 Oe, when the moment reaches about 2.2 μ_B/per Fe^{II} at 1.8 or 5 K. As the field increases, M increases in a quasi-linear fashion without saturation even at 50 kOe. Hysteresis loops are obtained at 15 K and below, with coercive fields up to 1000 Oe at 1.8 K.

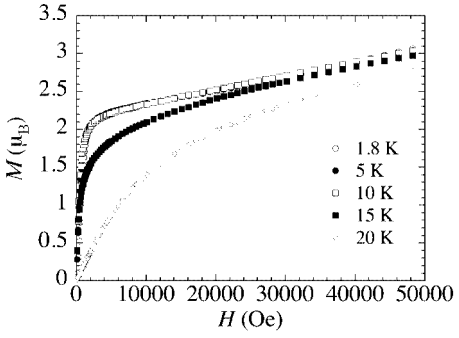

Figure 6. First magnetisation of the magnetic moment per Fe^{II} for α-FeFA·1/3HCO_2H

Fe(3) and Fe(4) each link to two Fe(1) chain centres via a single oxygen bridge (with Fe−O−Fe angles 111.84 or 113.54°) and two *syn*,*syn*-carboxylate bridges. Geometries corresponding to the interchain pathways have been previously observed in a small number of Fe^{II} complexes: $Ba_4(C_2O_4)Cl_2[\{Fe(C_2O_4)(\mu\text{-}OH)\}_4]$[28] which has an Fe−O−Fe angle of 122° and J/k_B = −9 K, $[Fe_2(\mu\text{-}OH)(\mu\text{-}OAc)_2(Me_3TACN)_2](ClO_4)$[29] (where Me_3TACN is 1,4,7-trimethyl-1,4,7-triazacyclononane) with an Fe−O−Fe angle of 113.2° and J/k_B = −18.7 K, $[Fe_2(\mu\text{-}OH)(\mu\text{-}Ph_3CCO_2)_2(Me_3TACN)_2](OTf)$[30] which displays an Fe−O−Fe angle of 119.1° and J/k_B = −17.4 K, and finally deoxyhemerythrin for which the Fe−O−Fe angle is not precisely known but for which J/k_B has been variously reported to be in the range −17 to −55 K[31] or as −21 K.[32] In all these compounds, the magnetic interactions are mediated by a single oxygen and two *syn, syn*-carboxylate bridges and have been found to be always antiferromagnetic. Due to the similarity of the geometries of these bridges to the interchain pathways in α-FeFA·1/3HCO_2H and in particular for the acetate-bridged dinuclear complex, these results enable us to conclude that our interchain linkages Fe(1)−Fe(3,4) are antiferromagnetic. Since the Weiss constant indicates that the dominant interactions in α-FeFA·1/3HCO_2H are ferromagnetic, the intrachain interaction must therefore be ferromagnetic and larger in magnitude than the antiferromagnetic interchain interaction. Unfortunately, to the best of our knowledge, no complex in which two Fe^{II} ions are linked via two oxygen bridges and one *syn, syn*-carboxylate bridge, which could confirm this conclusion, has been reported to date. However, based on this analysis, the magnetic structures of α-FeFA·1/3HCO_2H and MnFA[22b] are similar and composed of ferromagnetically-coupled Fe^{II} chains in which the magnetic moments are parallel and the linking Fe(3) and Fe(4) centres have antiparallel spins. Since the different metal centres occur in the ratio Fe(1):Fe(2):Fe(3):Fe(4) = 2:2:1:1 in the structure, this gives rise to the net magnetic moment. The saturation moment in the magnetic phase should thus be 1.6 μ_B per Fe^{II} or 9.8 μ_B per 6 Fe^{II}, based on g = 2.45 deduced from the high temperature susceptibility.

As shown in Figure 7, a rapid increase in the magnetisation with applied field is observed for low fields, as expected for a magnet. However, the magnetisation reaches 2.2 μ_B per Fe^{II} which is greater than the expected value of 1.6 μ_B. There are two possible causes for this behaviour which are not necessarily mutually exclusive: either the spins on Fe(3) and Fe(4) are not completely antiparallel to those on Fe(1) and Fe(2) or the g values for Fe(3) and Fe(4) might be smaller than for Fe(1) and Fe(2). In either or both cases, the magnetic moment of the magnetic phase is increased by an incomplete compensation of two of the four Fe(1,2) spins by the two Fe(3,4) spins. At higher fields (Figure 7) the magnetisation increases linearly with the applied magnetic field to reach ca. 3 μ_B per Fe^{II} at 5 T. This behaviour is consistent with the progressive alignment of the antiparallel magnetic spins on Fe(3,4) within the field. From the magnetic data discussed so far α-FeFA·1/3(HCO_2H), as for MnFA,[22b] can be understood in terms of ferromagnetic interactions within the chains and antiferromagnetic interchain interactions resulting in what can be described here, as in ref.[22b], as ferrimagnetic behaviour even though there is only one type of spin in the structure. This is in accordance with the definition of Néel that in a ferrimag-

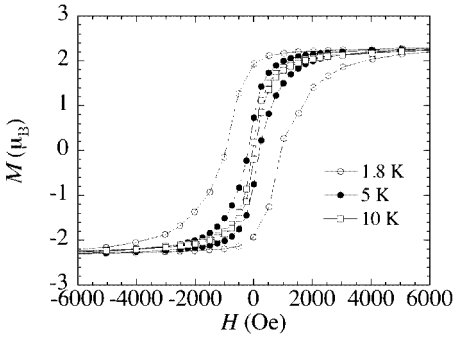

Figure 7. Hysteresis loops of the magnetic moment per Fe^{II} for α-FeFA·1/3HCO_2H obtained at a field sweep rate of 12 Oe/s

netic material, the magnetic moments of different sublattices do not compensate and a spontaneous magnetisation remains. For the iron complex, the ordering temperature T_c is 16 K and this is considerably higher than the maximum value of 8 K reported for the series of Mn^{II} compounds in ref.[22b]

To confirm this magnetic ordering, the temperature dependence of the in-phase (χ') and out-of-phase (χ'') magnetic susceptibilities have been measured (Figure 8). Both components exhibit a peak at 1 Hz at temperatures of 15 and 12 K for χ' and χ'', respectively. Independent of the frequency, χ'' becomes nonzero around 16 K in agreement with the ordering temperature already estimated by the heat capacity and *d.c.* measurements (vide supra). Closer analysis of the *a.c.* data reveals a slight frequency dependence for both the maximum and the breadth of the peaks. The positions of the χ' and χ'' peaks increase by less than 0.5 K and ca. 1.3 K, respectively, when the frequency is increased from 1 to 1500 Hz. Mydosh established that the frequency dependence of the *a.c.* measurements can quantify the degree of glassiness in a material by the parameter γ.[33] Such analysis of the data presented here leads to a γ value of 0.015, indicating that the magnetic order observed below 16 K involves a slight degree of glassiness.

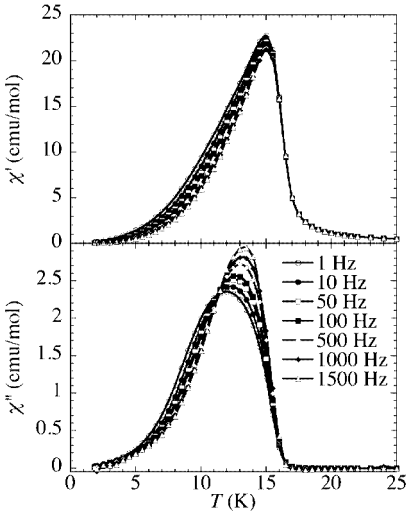

Figure 8. Temperature-dependence of the in-phase, χ', and out-of-phase, χ'', ac susceptibilities per Fe^{II} in α-$FeFA\cdot 1/3HCO_2H$ for a range of ac frequencies: dc field zero; ac field of amplitude 3 Oe

In contrast to the iron compound, the magnetic behaviour of the cobalt analogue is dominated by antiferromagnetic interactions and no magnetic order has been observed down to 1.8 K. The plot of χ^{-1} against T can be fitted (using data above 70 K) to the Curie−Weiss law with a Curie constant of 3.30 emu K mol^{-1} and a negative Weiss constant of −14.8 K. The Curie constant is in good agreement with typical values for high spin octahedral Co^{II} (S = 3/2).[27a] As indicated by the Weiss constant, dominant antiferromagnetic interactions are present between Co^{II} centres in α-$CoFA\cdot 1/3HCO_2H\cdot 1/3H_2O$. Nevertheless, a contribution from spin-orbit coupling of Co^{II} is also expected and probably enhances the Weiss constant extrinsically. In an octahedral ligand field the $^4T_{1g}$ ground state of the S = 3/2 Co^{II} metal ions is split by spin-orbit coupling into a set of three levels with an effective S = 1/2 ground state and leads to the possibility of large g values.[34]

Mössbauer Spectra

In order to investigate the relationship between electronic structure and magnetism in more detail, Mössbauer spectra of α-$FeFA\cdot 1/3HCO_2H$ were collected between 4 and 295 K (Figure 9). The spectra reflect the different iron sites in the crystal structure and are in agreement with the development of 3D magnetic order, as indicated by the pronounced changes in the shape of the spectra around 16 K (Figure 9).

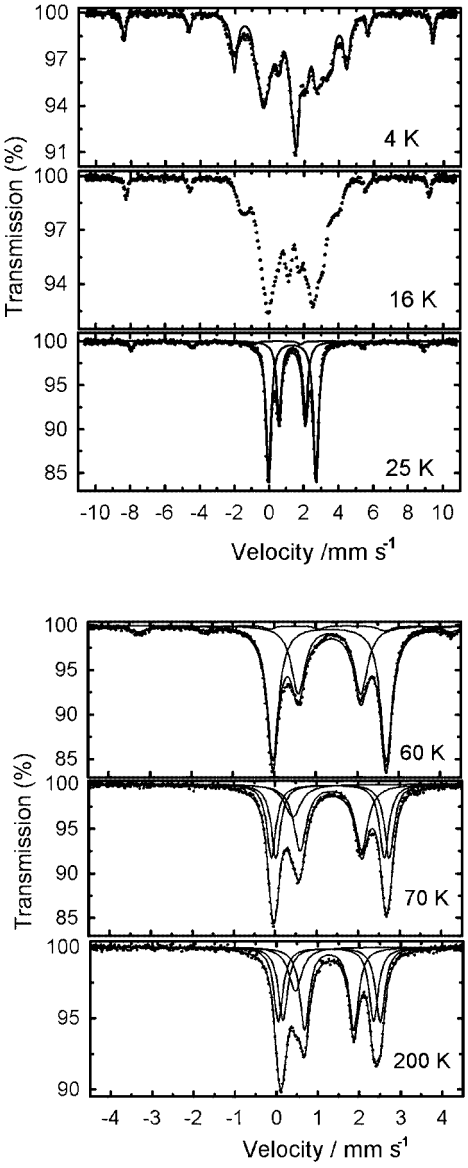

Figure 9. Mössbauer spectra of α-$FeFA\cdot 1/3HCO_2H$ in the temperature range of the magnetic phase transition (top) and in the paramagnetic phase (bottom); solid lines correspond to the best fits and the constituent subspectra

The spectra of the paramagnetic phase above 16 K (e.g. the 25 K spectrum) essentially consist of two quadrupole doublets with an intensity ratio of roughly 2:1. Their isomer shifts *IS* (see Table 5) are nearly identical and typical for high spin Fe^{2+} sites. From the relative intensities, the outer doublet with the larger quadrupole splitting ΔE_Q can be assigned to the chain Fe(1) and Fe(2) sites with the second doublet showing the smaller ΔE_Q corresponding to the bridging Fe(3) and Fe(4) atoms. In the spectrum at 25 K, in addition to the major component arising from the Fe^{2+} paramagnetic signals, a hyperfine sextet with an isomer shift and a hyperfine field B_{hf} typical of Fe^{3+} can be observed (Table 5). The six-line pattern indicative of a magnetically-ordered phase persists up to about 60 K above which it collapses into a broad single line. This subspectrum can be attributed to the presence of about 8% of the cubic Fe^{III} formate $Fe(O_2CH)_3{\cdot}HCO_2H$ (subsequently identified by X-ray powder diffraction) which becomes antiferromagnetically ordered near 60 K and will be described elsewhere.[28] Below 60 K only two of the six lines fall within the region of the spectrum of α-FeFA·1/3HCO_2H and their shapes can be determined accurately from the four falling outside this region so that fitting the α-FeFA·1/3HCO_2H spectrum was essentially unaffected by the presence of this impurity.

Table 5. Mössbauer parameters of α-FeFA·1/3HCO_2H in the paramagnetic region at selected temperatures; the Fe(1,2) sites are described by one quadrupole doublet at 25 K and two doublets [Fe(1,2) a and b] for $T \geq 70$ K, whereas the Fe(3,4) sites were always modelled by a single somewhat broadened quadrupole doublet; errors are less than 1 in the last digit if not given explicitly in parentheses

T (K)	site	IS (mm·s^{-1})	ΔE_Q (mm·s^{-1})	Rel. area (%)
25	Fe(1,2)	1.35	2.73	60
	Fe(3,4)	1.35	1.52	32
	Fe^{3+}	0.50	–	8
70	Fe(1,2)a	1.33	2.84	56[a]
	Fe(1,2)b	1.33	2.61	
	Fe(3,4)	1.35	1.48	33
	Fe^{3+}	0.43	–	11
295	Fe(1,2)	1.22	2.14	25(2)
	Fe(1,2)b	1.20	1.85	29(2)
	Fe (3,4)	1.21	1.00	34
	Fe^{3+}	0.40	–	12

[a] Total Fe(1,2) area. The areas of Fe(1,2)a and Fe(1,2)b were assumed to be equal.

A more detailed inspection of the spectra recorded in the paramagnetic region (Figure 9) revealed that the Fe(1) and Fe(2) sites in the crystal structure of α-FeFA·1/3HCO_2H can be distinguished since their quadrupole splittings are somewhat different. This is particularly apparent from the shape of the spectrum recorded at 200 K (the temperature of the crystal structure determination). Thus, the Fe^{2+} part of the spectrum was modelled by three doublets. Although the Fe(3,4) sites cannot be similarly resolved, a certain line broadening at low temperatures indicates slightly different quadrupole splittings. As expected for $3d^6$ high spin Fe^{2+} ions, ΔE_Q is temperature dependent (Figure 10) for the Fe(1,2) as well as for the Fe(3,4) sites reflecting the aspherical electron distribution arising from the splitting of the octahedral t_{2g} orbitals in the lower symmetry ligand field. The rather small value for ΔE_Q of ca. 1.5 mm·s^{-1} for the Fe(3,4) sites even at 25 K suggests that their electronic structures result from the orbital splitting of an elongated octahedron, in agreement with the structural data (vide supra) where the d_{xz} and d_{yz} orbitals are below the d_{xy} orbital.[35] In addition, the degeneracy of the d_{xz} and d_{yz} orbitals is likely to be lifted because the equatorial bond lengths are different. The much larger ΔE_Q for the Fe(1,2) sites suggests a different sequence of orbitals for these more distorted sites but a more detailed analysis would need to take the effects of spin-orbit coupling into account.

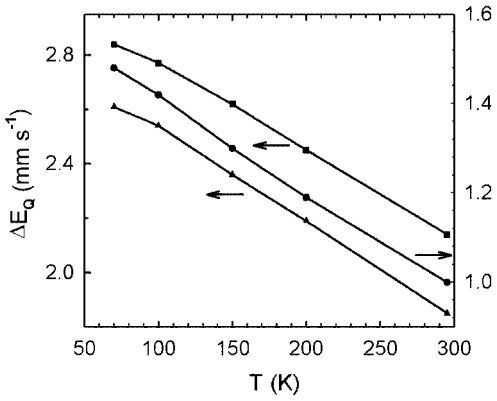

Figure 10. Temperature dependence of the quadrupole splitting for the Fe(1,2) sites (left scale) and the Fe(3,4) sites (right scale); solid lines are guides for the eye

The shape of the 4 K spectrum is completely different from that of the high temperature spectra and indicates that all the Fe^{2+} sites are magnetically ordered. Modelling of the spectrum is complicated by the fact that for Fe^{2+} compounds, electric quadrupole and magnetic hyperfine interactions are generally of comparable size and it is not possible to analyse the spectra in terms of six line patterns with an intensity ratio 3:2:1:1:2:3. Accordingly, the 4 K spectrum was modelled with the software package Recoil[36] employing the full static Hamiltonian for mixed hyperfine interactions with four Fe^{2+} sites and one Fe^{3+} site (to account for the impurity) included in the calculations. This data treatment resulted in a large number of parameters which cannot all be deduced unambiguously from powder spectra since each iron site is characterised by (i) its isomer shift *IS* (ii) the hyperfine field B_{hf} (iii) the quadrupole interaction parameter $\varepsilon = eQV_{ZZ}/2$ (where V_{ZZ} is the Z component of the diagonalised electric field gradient (efg) tensor, Q = quadrupolar moment of the iron nucleus) (iv) the asymmetry parameter η of the efg tensor ($0 \leq \eta \leq 1$) and (v) the polar and azimuthal angles Θ and Φ describing the orientation of $\mathbf{B_{hf}}$ in the efg principal axes coordinate system. For this reason it was assumed that the values for the *IS* and quadrupole splittings $\Delta E_Q = (V_{ZZ}Q/2)(1 + \eta^2/3)^{1/2}$

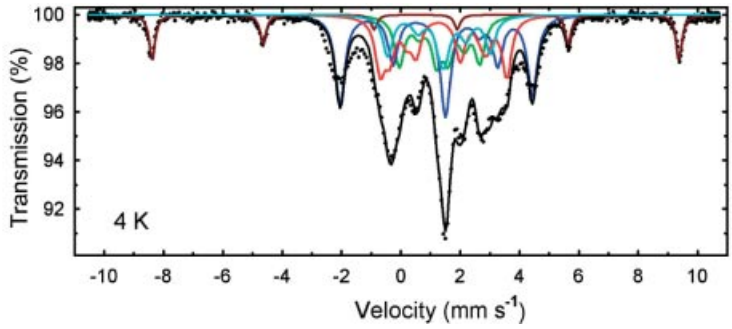

Figure 11. Analysis of the 4 K Mössbauer spectrum using the full Hamiltonian for combined quadrupole and magnetic hyperfine interactions; the black solid line corresponds to a theoretical spectrum obtained with the parameters given in Table 6; blue and red lines correspond to the Fe(1,2) subspectra, green and cyan lines to the Fe(3,4) subspectra; see text for more details

in the paramagnetic phase at 25 K and in the magnetically ordered phase at 4 K are identical. A reasonable description of the overall shape of the spectrum (Figure 11) was obtained with the parameters summarised in Table 6. In this model, the efg of the Fe(3,4) sites was assumed to be axially symmetric so that the spectra do not depend on the azimuthal angles Φ which were set to zero for these as well as for the Fe(1,2) sites. The negative value of V_{ZZ} for the Fe(3,4) sites is in agreement with an orbital doublet ground state. The best simulation of the overall shape of the spectrum was obtained also by using a negative value of V_{ZZ} for the Fe(1,2) sites, although a positive value cannot be ruled out. The experimental spectrum reveals considerable line broadening at higher velocities indicating a distribution of hyperfine fields. This was not taken into account in the data analysis and points to disorder effects which are also believed to be the origin of the frequency dependence of the *a.c.* susceptibility data (vide supra).

Table 6. Mössbauer parameters of α-$FeFA\cdot 1/3HCO_2H$ obtained from the analysis of the 4 K spectrum with the full hyperfine Hamiltonian; the full width at half maximum was set to 0.4 $mm\cdot s^{-1}$ for all Fe^{2+} sites and to 0.24 $mm\cdot s^{-1}$ for the Fe^{3+} site; the azimuthal angle Φ was kept at zero for all sites; Fe(1,2) and Fe(3,4) are split into two sites a and b, respectively

Site	IS ($mm\cdot s^{-1}$)	ε ($mm\cdot s^{-1}$)	η	B_{hf} (Tesla)	Θ (°)	rel. Area (%)
Fe(1,2)a	1.35[a]	−2.55[a]	0.6[b]	15.1	51	33
Fe(1,2)b	1.35[a]	−2.55[a]	0.6[b]	7.5	90	25
Fe(3,4)a	1.35[a]	−1.5[a]	0[b]	4.7	44	19
Fe(3,4)b	1.35[a]	−1.5[a]	0[b]	7.5	45	15
Fe^{3+}	0.50[a]	–	–	55.1	–	9

[a] Parameters taken from the 25 K spectrum. Note that $\Delta E_Q = (eQV_{ZZ}/2)(1 + \eta^2/3)^{1/2} = \varepsilon(1 + \eta^2/3)^{1/2}$. A negative sign for V_{ZZ} was assumed for both sites. [b] Parameter was not varied during fitting but analysis was performed for different η values.

The range of B_{hf} values found from this analysis for the various Fe sites in α-$FeFA\cdot 1/3HCO_2H$ (Table 6) is similar to those of other Fe^{2+} compounds.[37] The observed hyperfine field is a sum of three contributions:

$$B_{hf} = B_C + B_L + B_D$$

where B_C is the isotropic Fermi contact contribution and B_L and B_D correspond to the anisotropic dipolar interactions between the nuclear momentum and the electronic angular and spin momentum, respectively. According to a common rule of thumb,[38] the $S = 2$ state of Fe^{2+} can be expected to lead to a B_C value of roughly −44 T which is compensated by positive B_L and B_D contributions with B_L being dominant and proportional to the expectation value $<L>$ of the angular momentum. The value of $<L>$ and therefore B_L is expected to be larger for the more symmetric Fe(3,4) than for the more distorted Fe(1,2) sites implying that the sign of B_{hf} is negative for the Fe(1,2) and positive for the Fe(3,4) sites. The small hyperfine field values are evidence for the importance of the angular contribution to the magnetic moment for both kinds of Fe sites in the crystal structure of α-$FeFA\cdot 1/3HCO_2H$ and the resultant magnetic anisotropy will also influence the detailed spin structure in the magnetically ordered phase.

Finally, we note that the 16 K spectrum (Figure 9) corresponds to a superposition of magnetically ordered and paramagnetic phases in good agreement with a T_C value of 16 K derived from the magnetic susceptibility measurements. Mössbauer spectra in an external magnetic field could shed more light on the electronic structure and magnetic exchange interactions of the various Fe sites in the present compound and elastic neutron scattering studies would be a further means of probing the magnetic structures. However, based on what is already in the literature[22,29−33] and the complementary susceptibility and Mössbauer studies we have presented here, we feel that our proposed model for the spin structure is probably justified.

Conclusion

We have described the synthesis, structure and the magnetic properties of the mesoporous compound $Fe(HCO_2)_2\cdot 1/3HCO_2H$ which is a magnet below 16 K. As the member with the highest T_C of a newly-discovered family of M^{II} formate framework structures with high stabilities

and the ability to take up specific gas molecules, it points to a promising way forward in combining magnetic and porous properties which could find applications in separation techniques.

Experimental Section

FeFD, CoFD, NiFD, ZnFD and MgFD were synthesised as reported previously.[39]

Synthesis of α-$Fe(O_2CH)_2$·1/3HCO_2H: In a typical experiment $Fe(O_2CH)_2$·2H_2O (0.1 g, 0.5 mmol) was heated in formic acid (7 mL) to 70 °C in a steel autoclave with a Teflon-insert of internal volume 10 mL for a period of 8 hours. After slow cooling, α-FeFA·1/3HCO_2H was obtained in quantitative yield. The polycrystalline product was washed with formic acid, dried and stored under an inert atmosphere. The product was shown to be a single-phase by powder diffraction except in the case of the sample used for the Mössbauer measurements which contained about 8% of the Fe^{III} impurity $Fe(O_2CH)_3$·HCO_2H as described in the text.
Single-crystals of α-FeFA·1/3HCO_2H could obtained when formic acid was allowed to evaporate slowly under solvothermal conditions. $Fe(O_2CH)_2$·2H_2O (60 mg, 0.3 mmol) was heated in formic acid (8 mL) for 12 hours at 170 °C. The mixture was then cooled to 110 °C over 2 hours, maintained at this temperature for a further 28 hours then slowly cooled to room temperature. In this preparation, the autoclave lid was not closed tightly, allowing very slow loss of solvent from the autoclave.

Synthesis of α-$Co(O_2CH)_2$·1/3HCO_2H·1/3H_2O: The synthesis of polycrystalline material was as for α-FeFA·1/3HCO_2H. Single-crystals of α-CoFA·1/3HCO_2H·1/3H_2O could be obtained under solvothermal conditions by the modification described for α-FeFA·1/3HCO_2H. $Co(O_2CH)_2$·2H_2O (200 mg, 1 mmol) was heated in formic acid (4 mL) for 100 hours at 160 °C.

Synthesis of α-$Zn(O_2CH)_2$·1/3(HCO_2H): A quantitative yield of α-$Zn(O_2CH)_2$·1/3HCO_2H was obtained by recrystallisation of $Zn(O_2CH)_2$·2H_2O (4.88 g, 25.5 mmol) with formic acid (6 mL) at 120 °C for 120 hours. The autoclave lid was not closed tightly, allowing very slow loss of solvent from the autoclave.

Synthesis of α-$Ni(O_2CH)_2$·*x*HCO_2H·*y*H_2O: A 0.5 mm i.d. glass capillary tube was filled to a depth of 1 cm with $Ni(O_2CH)_2$·2H_2O and formic acid and was placed together with formic acid (2.5 mL) in the Teflon insert of the autoclave and heated at 170 °C for 17 hours. After cooling, the capillary tube was sealed and the X-ray powder pattern was measured.

Synthesis of α-$Mg(O_2CH)_2$·1/3HCO_2H: $Mg(O_2CH)_2$·2H_2O (1.22 g, 16.2 mmol) and formic acid (2 mL) were heated for 105 hours to 120 °C. The resultant polycrystalline powder was separated from the solvent by filtration and dried in air.

Single-Crystal X-ray Diffraction Studies: Data were measured on Stoe IPDS or Stoe IPDS II image plate area detector diffractometers using graphite-monochromated Mo-*Kα* radiation (λ = 0.71073 Å). Structures were solved by direct methods and refined by full-matrix least-squares against F^2 (all data) using the SHELXTL software package.[40] Nonhydrogen atoms were assigned anisotropic thermal parameters. Hydrogen atoms were fully refined with isotropic temperature factors (Co and Zn) or positionally refined with U set at 1.2U_{eq} for the carbon atom (Fe). Crystal data and experimental details are summarised in Table 1. CCDC-238105 to -238107 contain the supplementary crystallographic data for this paper. These data can be obtained free of charge from The Cambridge Crystallographic Data Centre via www.ccdc.cam.ac.uk/data_request/cif.

X-ray Powder Diffraction: X-ray powder patterns were measured at ambient temperature on a Stoe STADI-P diffractometer using Co-$K\alpha_1$ radiation (Ge monochromator) and Debye−Scherrer geometry. The sample was held between sheets of amorphous polyacetate foil. Data analysis was carried out with the WinXPow 1.07 software suite.
The unit cell for α-$Ni(O_2CH)_2$·*x*HCO_2H·*y*H_2O was determined from powder diffraction measurements made on the ANKA-DIFF beamline at the ANKA synchrotron source at the Forschungszentrum Karlsruhe at ambient temperature and using radiation of wavelength 1.58845(3) Å.

Thermal Analyses: The differential thermal analyses (DTA) and the thermogravimetric (TG) experiments were carried out using a Netzsch STA 409C system. Samples were heated in Al_2O_3 crucibles with a heating rate of 1 K min^{-1} up to 600 °C under a nitrogen atmosphere with a flow rate of 30 L h^{-1}.

Susceptibility Measurements: The magnetic susceptibility measurements were obtained with the use of a Quantum Design SQUID magnetometer MPMS-XL. Measurements were performed on finely ground polycrystalline samples of α-FeFA·1/3HCO_2H (13.13 mg) and α-CoFA·1/3HCO_2H·1/3H_2O (5.1 mg) in the temperature range 1.8−300 K with fields up to 7 T. The magnetic data were corrected for the sample holder and the diamagnetic contribution calculated from Pascal's constants.[41]

^{57}Fe Mössbauer Spectroscopy: Temperature dependent Mössbauer spectra of powdered samples of α-FeFA·1/3HCO_2H (about 10 mg natural iron per cm^2 with the samples diluted with polyethylene to ensure homogeneous distribution of the sample in the plexiglass container) were measured in an Oxford flow cryostat with a conventional Mössbauer spectrometer operating with a sine-type drive signal. All spectra were referenced to α-Fe.

Heat Capacity Measurements: The heat capacity measurements were performed on a Quantum Design PPMS system. A pressed pellet of the sample was mounted using grease on the heat capacity sample holder.

IR Spectroscopy: FTIR spectra were measured using KBr pellets of the sample in the range from 4000 to 400 cm^{-1} with a Perkin−Elmer Spectrum One instrument.

Acknowledgments

We acknowledge the ESF "Molecular Magnets" program for funding the short scientific stays of Rodolphe Clérac. R.C. thanks the CNRS, the University of Bordeaux 1 and the Conseil Regional d'Aquitaine for financial support. M. V., P. A., C. E. A. and A. K. P. thank the DFG Centre for Functional Nanostructures (CFN) for financial support. We thank W. Hölle for technical assistance with the measurement of the Mössbauer spectra performed at the Max-Planck-Institut für Festkörperforschung, Stuttgart. We thank Stephen Doyle for the measurement of the high resolution X-ray powder data at the ANKA-DIFF beamline, Forschungszentrum Karlsruhe.

[1] R. D. Cannon, R. P. White, *Prog. Inorg. Chem.* **1988**, *36*, 195−298.

[2] T. Lis, *Acta Crystallogr., Sect. B* **1980**, *36*, 2042−2046.

[3] [3a] H. J. Eppley, H.-L. Tsai, N. de Vires, K. Folting, G. Christou, D. N. Hendrikson, *J. Am. Chem. Soc.* **1995**, *117*, 301−317. [3b] S. M. J. Aubin, Z. Sun, I. A. Guzei, A. L. Rheingold, G. Christou, D. N. Hendrikson, *Chem. Commun.* **1997**, 2239−2240.

[4] [4a] Z. A. D. Lethbridge, A. D. Hiller, R. Cywinski, P. Lightfoot, *J. Chem. Soc., Dalton Trans.* **2000**, 1595−1599. [4b] P. A. Prasad, S. Neeraj, S. Natarajan, C. N. R. Rao, *Chem. Commun.* **2000**, 1251−1252. [4c] Z. A. D. Lethbridge, S. K. Tiwary, A. Harrison, P. Lightfoot, *J. Chem. Soc., Dalton Trans.* **2001**, 1904−1910.

[5] J. D. Martin, R. F. Hess, *Chem. Commun.* **1996**, 2419−2420.

[6] [6a] L. G. Beauvais, J. R. Long, *J. Am. Chem. Soc.* **2002**, *124*, 12096−12097. [6b] M. Cavellec, D. Riou, C. Ninlaus, J.-M. Grèneche, G. Férey, *Zeolites* **1996**, *17*, 250−260. [6c] M. Cavellec, D. Riou, C. Ninlaus, J.-M. Grèneche, G. Férey, *Magn. Magn. Mater.* **1996**, *163*, 173−183. [6d] X. X. Zhang, S. S.-Y. Chui, I. D. Williams, *J. Appl. Phys.* **2000**, *87*, 6007−6009. [6e] N. Guillou, Q. Gao, P. M. Forster, J.-S. Chang, M. Noguès, S.-E. Park, G. Férey, A. K. Cheetham, *Angew. Chem. Int. Ed.* **2001**, *40*, 2831−2834. [6f] A. Rujiwatra, C. J. Kepert, J. B. Claridge, M. J. Rosseinsky, H. Kumagai, M. Kurmoo, *J. Am. Chem. Soc.* **2001**, *123*, 10584−10594. [6g] K. Barthelet, J. Marrot, D. Riou, G. Férey, *Angew. Chem. Int. Ed.* **2002**, *41*, 281−284.

[7] M. Viertelhaus, *Darstellung und Charakterisierung wasserfreier Metall(II)- und Metall(III)formiate*, Mensch und Buch Verlag, Berlin, **2003**.

[8] K. Osaki, Y. Nakai, T. Watanabe, *J. Phys. Soc. Jap.* **1963**, *18*, 919.

[9] F. Sapina, M. Burgos, E. Escrivá, J.-V. Folgado, D. Marcos, A. Beltrán, D. Beltrán, *Inorg. Chem.* **1993**, *32*, 4337−4344.

[10] G. Weber, *Acta Crystallogr., Sect. B* **1980**, *36*, 1947−1949.

[11] M. Viertelhaus, H. Henke, C. E. Anson, A. K. Powell, *Eur. J. Inorg. Chem.* **2003**, 2283−2289.

[12] D. Dollimore, J. P. Gupta, D. V. Nowell, *Thermochim. Acta* **1979**, *30*, 339−350.

[13] R. C. Eckhardt, T. B. Flanagan, *Trans. Faraday Soc.* **1964**, *60*, 1289−1298.

[14] C. Malard, *C. R. Acad. Sc. Paris Ser. C* **1966**, *263*, 480−483.

[15] T. Arii, A. Kishi, *Thermochim. Acta* **1999**, *325*, 157−165.

[16] G. Périnet, *Bull. Soc. Franc. Minér. Crist.* **1966**, *89*, 325−328.

[17] T. Arii, A. Kishi, Y. Kobayashi, *Thermochim. Acta* **1999**, *325*, 151−156.

[18] P. Baraldi, *Spectrochim. Acta A* **1979**, *35*, 1003−1007.

[19] [19a] R. C. Eckhardt, P. M. Fichte, T. B. Flanagan, *Trans. Faraday. Soc.* **1971**, *67*, 1143−1154. [19b] Y. Masuda, M. Hatakeyama, *Talanta* **1996**, *43*, 1705−1709. [19c] Y. Masuda, M. Hatakeyama, *Thermochim. Acta* **1998**, *308*, 165−170.

[20] E. Kalalova, V. Ruzicka, *Coll. Czech. Chem. Commun.* **1962**, *27*, 424−429.

[21] V. Z. Vassileva, A. L. Karapetkova, *Bulg. Chem. Commun.* **1995**, *28*, 151−159.

[22] [22a] D. N. Dybtsev, H. Chun, S. H. Yoon, D. Kim, K. Kim, *J. Am. Chem. Soc.* **2004**, *126*, 32−33. [22b] Z. Wang, B. Zhang, H. Fujiwara, H. Kobayashi, M. Kurmoo, *Chem. Commun.* **2004**, 416−417.

[23] C. Malard, *C. R. Acad. Sc. Paris Ser. C* **1966**, *263*, 480−483.

[24] Unpublished results.

[25] A. L. Spek, *PLATON − A Multipurpose Crystallographic Tool*, Utrecht University, Utrecht, The Netherlands, **2002**.

[26] K. Nakamoto, *Infrared and Raman Spectra of Inorganic and Coordination Compounds. Part B: Applications in Coordination, Organometallic and Bioinorganic Chemistry*, John Wiley & Sons, New York, **1997**.

[27] [27a] F. E. Mabbs, D. J. Machin, *Magnetism and Transition Metals Complexes*, Chapman and Hall Ltd., London, **1973**. [27b] R. L. Carlin, *Magnetochemistry*, Springer-Verlag, Berlin, Heidelberg, **1986**.

[28] D. J. Price, S. Tripp, A. K. Powell, P. T. Wood, *Chem. Eur. J.* **2001**, *7*, 200−208.

[29] J. R. Hartman, R. L. Rardin, P. Chaudhuri, K. Pohl, K. Wieghardt, B. Nuber, J. Weiss, G. C. Papefthymiou, R. B. Frankel, S. J. Lippard, *J. Am. Chem. Soc.* **1987**, *109*, 7387−7396.

[30] S. C. Payne, K. S. Hagen, *J. Am. Chem. Soc.* **2000**, *122*, 6399−6410.

[31] R. C. Reem, E. I. Solomon, *J. Am. Chem. Soc.* **1987**, *109*, 1216−1226.

[32] M. J. Maroney, D. M. Kurtz, J. N. Nocek, L. L. Pearce, L. Que Jr., *J. Am. Chem. Soc.* **1986**, *108*, 6871−6879.

[33] J. A. Mydosh, *Spin Glasses: An Experimental Introduction*, Taylor and Francis, London, **1993**, p. 64.

[34] R. L. Carlin, *Magnetochemistry*, Springer-Verlag, **1986**.

[35] H. T. Le Fever, R. C. Thiel, W. J. Huiskamp, W. J. M de Jonge, *Physica B* **1981**, *111*, 190−208.

[36] K. Lagarec, D. G. Rancourt, Mössbauer Analysis Software Recoil (1.05).

[37] [37a] K. Ono, A. Ito, *J. Phys. Soc., Jpn.* **1964**, *19*, 899−907. [37b] S. G. Carling, D. Visser, D. Hautot, I. D. Watts, P. Day, J. Ensling, P. Gütlich, G. J. Long, F. Grandjean, *Phys. Rev. B* **2002**, *66*, 104407/1−104407/12.

[38] N. N. Greenwood, T. C. Gibb, *Mössbauer Spectroscopy*, Chapman and Hall, London, **1971**; p. 103.

[39] [39a] K. Nargorny, J. F. March, *Z. Phys. Chem.* **1972**, *78*, 311−316. [39b] V. Zapletal, J. Jedlick, V. Ruzicka, *Coll. Czech. Chem. Commun.* **1957**, *22*, 171−174.

[40] G. M. Sheldrick, *SHELXTL 5.1*, Bruker AXS Inc., 6300 Enterprise Lane, Madison, WI 53719−1173, USA, **1997**.

[41] *Theory and Applications of Molecular Paramagnetism* (Eds.: E. A. Boudreaux, L. N. Mulay), John Wiley & Sons, New York, **1976**.

[42] J. D. Donaldson, J. F. Knifton, S. D. Ross, *Spectrochim. Acta* **1964**, *20*, 847−851.

Received May 13, 2004

